EDGE ARTICLE

Check for updates

All publication charges for this article have been paid for by the Royal Society of Chemistry

Unveiling bulk-to-interface electrolyte regulation for ultralong-life Zn-ion batteries

Yinyan Deng, Shuangtao Xu, Zhiping Peng, Linfeng Fei [ID] * and Tao Wang*

Unsatisfactory Zn^{2+}/Zn interfacial behavior together with parasitic side reactions on the Zn anode are key issues limiting the cycling stability of aqueous zinc-ion batteries (AZIBs). To address these issues, electrolyte additives have been extensively explored, yet their efficacies are often unsatisfactory due to unknown structure-performance relationships or diverse trade-off effects. Herein, a carboxybetaine oligomeric additive, OCBA, is demonstrated to exhibit comprehensive regulation, from the bulk electrolyte to the electrode interface. Through theoretical calculations and experimental investigations, we find that strong interactions between OCBA and water/Zn^{2+}/Zn metal bring about the simultaneous promotion of ion migration either in the electrolyte or across the interface, elimination of Zn dendrite growth, deposition of Zn along the (002) facets, and suppression of hydrogen evolution and inactive byproducts. Remarkably, benefiting from this synergistic regulation, Zn//Zn cells achieve an ultralong lifespan of over 6660 h at 1 mA cm^{-2} and 1 mAh cm^{-2}, while Zn//Cu cells deliver a high Coulombic efficiency of 99.7% for $\approx$3000 cycles. Furthermore, Zn//polyaniline full cells show excellent rate performance and cycling stability. This study reveals the working mechanism of electrolyte additives and provides an effective strategy for developing high-performance AZIBs by additive design.

Introduction

Rechargeable aqueous metal-ion batteries exhibit great potential in megawatt- and kilowatt-scale energy storage applications due to their low cost, high safety levels, and environmental friendliness.[1–3] Aqueous zinc-ion batteries (AZIBs) are considered among the most promising candidates because of the intrinsic advantages of the zinc metal anode, including the relatively low redox potential (-0.76 V *vs.* SHE), high theoretical capacity (820 mAh g^{-1} or 5855 mAh cm^{-3}), and abundant resource availability.[4–6] However, the commercialization of AZIBs is still largely hindered by their poor Coulombic efficiency (CE) and limited cycling lifespans.[7–9]

The unsatisfactory performances of AZIBs mainly stem from the interfacial instability and complex side reactions on the electrodes.[10–12] In particular, for the anode side, dendrite growth, corrosion, continuous hydrogen evolution reaction (HER), and Zn^{2+} passivation at the Zn/electrolyte interface seriously jeopardize the cycling stability.[13,14] The plating/stripping of Zn is primarily governed by the overall process of Zn^{2+} transfer from the bulk solution to the electrode interface; specifically, the electrode interface refers to the electric double layer (EDL), including a diffuse layer (DL), an outer Helmholtz plane (OHP), and an inner Helmholtz plane (IHP).[15–17] On the

one hand, during the plating process, hydrated Zn^{2+} ions move from the bulk electrolyte to the DL, then the OHP, and finally the IHP for reduction and deposition. In this case, promoted Zn^{2+} migration in the electrolyte leads to a fast replenishment in the amount of Zn^{2+} in the DL and OHP to relieve the cation depletion, thereby facilitating dense Zn deposition.[18] Also, a reduced dehydration energy barrier of Zn^{2+} results in improved deposition kinetics of Zn.[19] Besides, controllable Zn deposition along specific crystal facets (*e.g.* (001)) effectively inhibits dendrite formation and electrode corrosion.[20] In summary, the uniform electrodeposition and stable cycling of Zn can be achieved with the synergy of the above factors. On the other hand, the IHP contains a certain number of H_2O molecules, which are inevitably reduced along with the electrodeposition; this leads to an increase of the HER as well as electrode corrosion.[21–23] Notably, OH^- from the water decomposition induces the formation of inactive byproducts Zn_a-$X(OH)_b$ (X represents an anion), which obstruct the reversible deposition/stripping of Zn^{2+}. Therefore, a reduced number of water molecules in the IHP should suppress the undesirable side reactions (HER, inactivation of anode, *etc.*).[17,23]

It is therefore crucial to provide comprehensive regulation for the electrolyte (*i.e.* from the bulk to the interface) for ideal interfacial behavior of Zn^{2+}/Zn; the regulation not only affects the concentration distribution of Zn^{2+} and charge transfer across the interfaces (which determines the nucleation behavior of Zn), but also eliminates water-induced parasitic side reactions (which in turn boosts the reversibility and long-term stability of the zinc

Department of Polymer Materials and Engineering, School of Physics and Materials Science, Nanchang University, Nanchang 330031, China. E-mail: feilinfeng@gmail.com; wangt0715@ncu.edu.cn

anode). In this regard, the use of functional electrolyte additives is widely recognized as one of the most appealing strategies to meet this goal.[10,21,22,24] A series of electrolyte additives have been proposed for extending the lifespan of AZIBs,[25,26] by coordinating with free water molecules or ions,[26] regulating the anode interface by electrostatic shielding or the steric effect,[8,27] or forming a solid electrolyte interphase (SEI).[28,29] Nevertheless, this strategy still faces fundamental challenges in terms of the biased and insufficient regulation effects of available additives. For instance, some additives are capable of regulating the structure of the EDL for eliminating dendrites and the HER, but Zn^{2+} migration in the bulk or across the interface can remain sluggish, or *vice versa*.[30] Additionally, although the modulation on the IHP can produce positive impacts on the plating process, recent studies suggest that an additive-modulated interface with dynamic adsorption behavior instead of a rigid additive layer in the EDL is much preferred for a long lifespan.[29,31,32] Therefore, it is urgent to explore the intrinsic regulation mechanisms for electrolyte additives.

Notably, zwitterionic electrolyte additives have exhibited great potential in improving the performance of AZIBs.[28,29,32,33] Considering the structural variations of zwitterionic moieties, their hydration ability and favorable interactions with Zn/Zn^{2+} are easy to tune;[34] accordingly, zwitterionic additives can deliver different capabilities or mechanisms in regulating the electrochemical behavior of AZIBs. Therefore, they are ideal candidates to eliminate the diverse trade-off effects of additives. In this work, a carboxybetaine (CBA) is compared with a sulfobetaine (PDP) through theoretical calculations on the chemistry of zwitterionic additives and their interactions with the electrolyte components. Subsequently, as recent reports have shown that polymeric/oligomeric zwitterions should have a chance to be optimized as multipotent additives due to the cooperative interactions among adjacent repeating units,[31] oligomeric additives (OCBA and OPDP) are compared in experimental investigations. Conclusively, OCBA is demonstrated as a superior electrolyte additive of AZIBs. Through tailored interactions with water and ions *via* its excellent hydration ability and high charge density, OCBA improves the electrochemical stability of water, boosts the migration of Zn^{2+}, and reduces the energy barrier of Zn^{2+} desolvation. Simultaneously, the strong affinity between OCBA and metallic Zn reduces the HER and inactive byproducts, and its dynamic adsorption behavior facilitates ion transfer across the interfaces. Consequently, Zn//Zn symmetric cells with the OCBA-based electrolyte demonstrate a remarkably prolonged cycling lifespan exceeding 6660 h (>9 months), and OCBA-based Zn//Cu asymmetric cells maintain a high average CE of 99.7% for ≈3000 cycles. Moreover, Zn//polyaniline (PANI) full cells exhibit superior rate performance and cycling stability with a capacity retention of 74.5% after 2000 cycles at 3 A g^{-1}. This work provides theoretical guidance and a practical basis for designing high-performance electrolyte systems.

Results and discussion

Simulations of the effects of additives from the bulk electrolyte to the interface

Zwitterionic additives have shown great capability in optimizing AZIBs toward high-performance and prolonged lifespans.[33,35] It has been discussed that zwitterionic groups can interact with water to reduce its activity,[18,28] coordinate with Zn^{2+} to increase ion migration,[36] or attach to Zn metal to reduce side reactions at the interfaces.[29,37] Therefore, to synergistically strengthen all the above interactions, an optimal design of zwitterionic structures is very promising. Zwitterions are typically divided into carboxybetaine, sulfobetaine, and phosphobetaine; carboxylate on carboxybetaine is regarded as a type of zincophilic functional group, and considered to have a higher charge density.[38] To investigate the regulation mechanism of the interfacial behavior of the zinc anode by different zwitterionic structures, two zwitterionic monomers are compared here, including a sulfobetaine (PDP) and a carboxybetaine (CBA). Their synthesis and characterization are demonstrated in Fig. S1–S4. Phosphobetaine is not adopted because of its opposite dipole direction.

The coordination situations of zwitterionic groups with Zn^{2+}, H_2O, or Zn metal were first analyzed by theoretical calculations. As shown in Fig. 1a, the carboxylate anion in CBA exhibits lower molecular electrostatic potential (ESP) values compared to the sulfonate anion in PDP. This is consistent with a previous report showing that carboxylate possesses a higher charge density than sulfonate,[38] implying the stronger coordination capability with Zn^{2+} for CBA. As shown in Fig. 1b, the binding energies among Zn^{2+}, zwitterions, and H_2O were compared based on density functional theory (DFT) calculations. The binding energies between Zn^{2+} and zwitterionic groups are significantly higher than that of Zn^{2+}–H_2O. This indicates that Zn^{2+} preferentially coordinates with the zwitterionic additives rather than with H_2O; accordingly, zwitterionic groups can enter the hydration shell of Zn^{2+} to partially substitute H_2O. Similarly, it was previously confirmed by in-depth molecular dynamics simulations that PDP can enter the hydration shell of Zn^{2+}.[29] In comparison, the binding between Zn^{2+} and –COO^- is stronger than that between Zn^{2+} and –SO_3^-, demonstrating the higher coordination efficacy of CBA for Zn^{2+} than that of PDP. Also, the binding energies between H_2O and the zwitterionic groups (–SO_3^- and –COO^-) are much higher than that of H_2O–H_2O, verifying the strong hydration ability of zwitterionic groups that can effectively disrupt the hydrogen network of water to enhance the electrochemical stability of H_2O.

ESP maps were further employed to reveal the differences in the Zn^{2+} solvation shell structures (Fig. 1c). Upon introducing a zwitterionic unit (CBA or PDP) into the primary solvation shell of Zn^{2+} to replace one water molecule, the ESP values around Zn^{2+} significantly decrease, suggesting a reduction in electrostatic repulsion between the ions. This is beneficial to Zn^{2+} ion transport, particularly the transport from the DL to OHP for relieving the concentration polarization at the interface. One should note that the incorporation of CBA through the –COO^- group results in a more extensively reduced ESP value compared with that of PDP through –SO_3^-, demonstrating a stronger ability of CBA in regulating the solvation environment of Zn^{2+}.

Then, prior to receiving electrons (*i.e.* to be reduced), Zn^{2+} needs to desolvate within the OHP and the desolvation is often the rate-determining step in the electrochemical deposition of Zn.[10] The additives that provide a synergistic way to reduce the
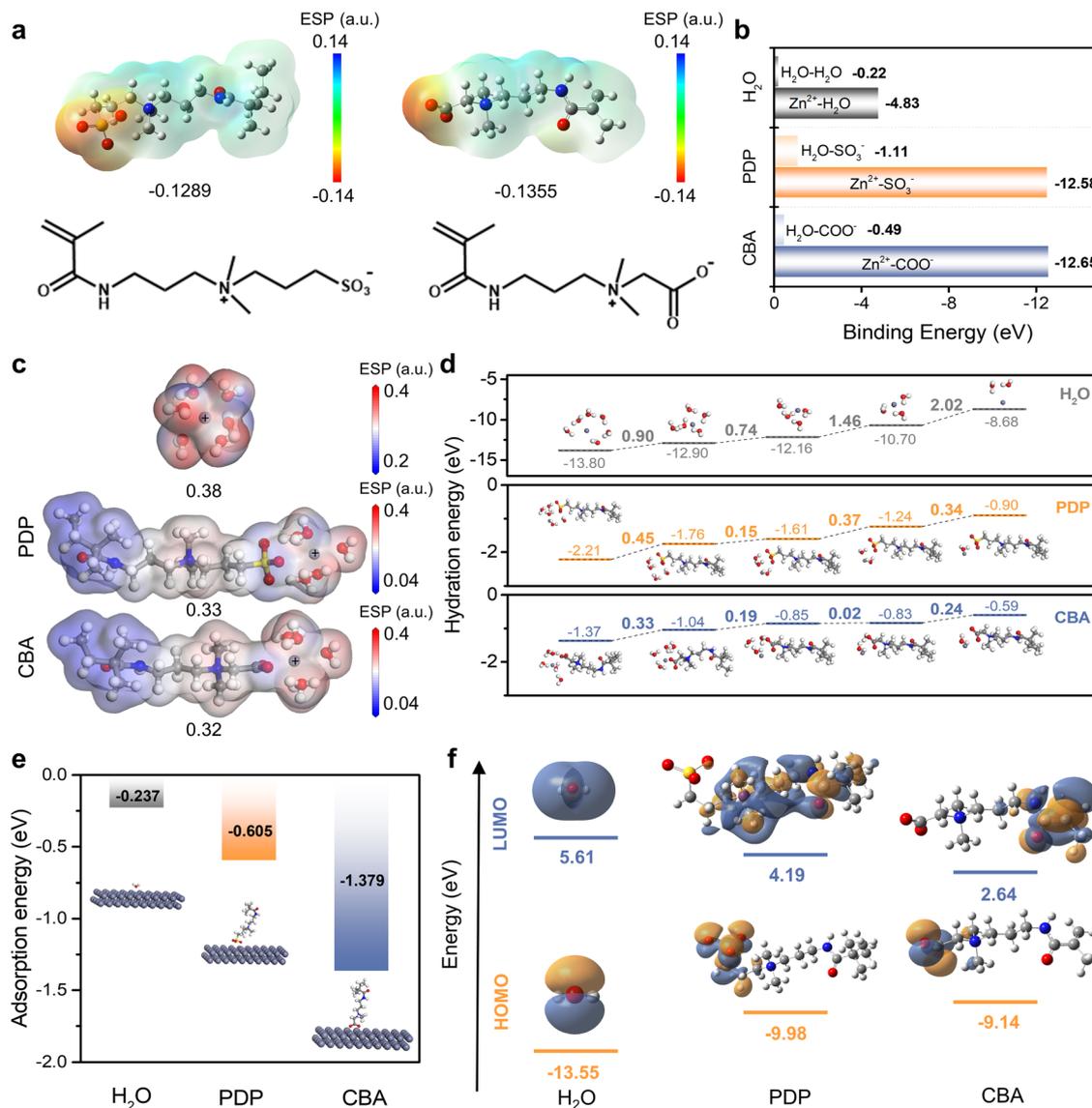
Fig. 1 Calculations of the effects of additives from the bulk electrolyte to the interface. (a) ESP distributions of PDP and CBA. (b) Binding energies of Zn^{2+} to H_2O, H_2O to H_2O, H_2O to $-SO_3^-$, Zn^{2+} to $-SO_3^-$, H_2O to $-COO^-$, and Zn^{2+} to $-COO^-$. (c) ESP maps of $Zn^{2+}-6H_2O$, $PDP-Zn^{2+}-5H_2O$, and $CBA-Zn^{2+}-5H_2O$. (d) Hydration energies of Zn^{2+} coordinated with H_2O, PDP, and CBA molecules. (e) Adsorption energies of H_2O, PDP, and CBA on the Zn (002) surface. (f) HOMO and LUMO energy levels of H_2O, PDP, and CBA.

desolvation energy of Zn^{2+} (E_a) can promote the charge/discharge kinetics of the electrode.[39] DFT calculations demonstrate that the desolvation process is more energetically favorable with the presence of CBA (Fig. 1d). Additionally, the IHP of the EDL can also be regulated through the specific adsorption of the additive on the electrode surface, which can inhibit the HER and modulate the interphase chemistry on the electrode.[21] Therefore, the adsorption of CBA and PDP at the Zn/electrolyte interface was further compared. As shown in Fig. 1e, DFT calculations reveal that the adsorption energies of the repeating units of PDP and CBA on the Zn (002) surface were −0.605 eV and −1.379 eV, respectively; both values are significantly higher than that of H_2O (−0.237 eV), indicating a stronger affinity of the zwitterionic additives for the Zn surface than water. This

strong interaction enables these additives to effectively replace H_2O molecules within the EDL, therefore suppressing interfacial side reactions. Moreover, the CBA unit again exhibits a much higher adsorption energy compared to the PDP unit, suggesting the preferential adsorption of CBA at the Zn/electrolyte interface for reconstructing the EDL.

Finally, as shown in Fig. 1f, the band gaps between the lowest unoccupied molecular orbital (LUMO) and the highest occupied molecular orbital (HOMO) energy levels of H_2O, PDP, and CBA were calculated as 19.16 eV, 14.17 eV, and 11.78 eV, respectively. According to molecular orbital theory, the higher HOMO of CBA indicates its higher propensity to lose electrons upon adsorption on the zinc surface, leading to the formation of a stable adsorption layer with zwitterionic groups. On the other side, the

lower LUMO of CBA demonstrates its higher priority in receiving electrons compared to PDP and H_2O, thereby mitigating water decomposition and assisting the SEI formation on the Zn anode.[10,40] Based on the above calculation results, zwitterionic additives based on the CBA unit represent all-in-one capability to realize comprehensive regulation from the bulk electrolyte to the interface, which is conducive to highly stable interfacial chemistry on the Zn metal anode.

Evolution of the bulk electrolyte and interfaces with additives

The two zwitterionic monomers were then polymerized to obtain oligomers with similar degrees of polymerization (D_p) for further experimental studies (OCBA and OPDP, Fig. S1). An oligomeric additive instead of a polymer was designed in terms of the requirement for a dynamic and even adsorption layer based on our previous report.[29] The influences of oligomer additives on the properties of the bulk electrolyte were first demonstrated. The OCBA additive results in a lower viscosity compared to OPDP for the electrolyte (Fig. S5, in which ZSO denotes $ZnSO_4$, and BE represents the bare electrolyte of 2 M $ZnSO_4$). Compared to carboxybetaine, the stronger hydration ability of sulfobetaine provides the OPDP chain with a larger hydrodynamic volume, therefore increasing the flow resistance of the electrolyte solution.[38] This low viscosity feature of OCBA is helpful in accelerating ion transport and electrolyte infiltration on electrodes. As shown in Fig. S6, as expected, the ionic conductivity of the electrolyte gradually decreases with the stepwise addition of OCBA due to the obstruction by molecular chains of ion migration.[41] Nevertheless, OCBA still demonstrates superiority compared to OPDP in the ionic conductivity of the electrolyte (see the comparison at the same additive concentration of 2 wt%); this higher conductivity is beneficial to alleviating the depletion of Zn^{2+} in the EDL of the anode during the Zn electrodeposition process, therefore restraining overpolarization and eliminating dendrite growth.

As a higher pH for the electrolyte is more favorable to suppress the HER,[42] the pH regulation of the additives for the electrolyte was subsequently analyzed. In the BE, Zn^{2+} coordinates with OH^- to produce the sparingly soluble byproduct $Zn(OH)_2$ and to result in the accumulation of H^+, so that the solution exhibits acidity (Fig. S7). Compared to the BE, the addition of OCBA can increase the pH of the electrolyte. This can be attributed to the coordination of the $-COO^-$ group on OCBA with Zn^{2+}, which reduces the reaction tendency of Zn^{2+} with OH^-. This buffering ability of OCBA is beneficial for alleviating the inactive byproduct. In this respect, the effectiveness of OPDP is lower than that of OCBA due to their different coordination abilities with Zn^{2+}, which is consistent with the above results from calculations. Additionally, pH stability is also important for inhibiting the inactive Zn^{2+} product and electrode corrosion during the interfacial reaction process. Buffer titration experiments were conducted in the presence of OCBA or OPDP, by recording the pH changes of the electrolyte upon gradually adding 0.1 M NaOH or 0.5 M H_2SO_4. As displayed in Fig. S8, the pH values of the three electrolytes all increase with the addition of NaOH, and display a downtrend

with the stepwise addition of H_2SO_4. Clearly, in the presence of OCBA, the pH changes were significantly restrained compared to those for the other two electrolytes, demonstrating the excellent capacity of OCBA for buffering pH fluctuations.

The amount of electrolyte additive was next optimized, as an overly low additive content may not be sufficient to regulate the electrochemical behavior of Zn^{2+}, while an excessively high additive content can induce an excessive reduction in conductivity and trigger a large voltage polarization. The effect of OCBA content on the Zn deposition/stripping behavior was tested in Zn//Cu half cells at a current density of 5 mA cm^{-2} and a capacity of 5 mAh cm^{-2} for electrolyte ingredient optimization (Fig. S9). Clearly, the Zn//Cu cell with 2 wt% OCBA/ZSO maintained an ultra-high average CE of 99.33% for more than 500 cycles. Accordingly, 2 wt% OCBA was selected as the optimal concentration for subsequent investigations. In contrast, 2 wt% OPDP/ZSO resulted in a much poorer lifespan of ≈ 100 cycles.

The interplay between the additives and Zn^{2+} was explored *via* NMR spectroscopy. As shown in Fig. 2a, in the ^{13}C NMR spectra, compared to the pure OCBA solution, the addition of 2 M $ZnSO_4$ distinctly induces the shift of the carbon resonance signal of $-COO^-$ in OCBA from 169.03 ppm to 169.65 ppm, generating a large chemical shift change ($\Delta\delta$) of 0.62 ppm. Meanwhile, the chemical shifts of hydrogen atoms on the CH_2 and CH_3 near the $-COO^-$ group both move to larger values (Fig. S10). For instance, the chemical shift of the hydrogen atoms of $-CH_2-COO^-$ showcases a positive $\Delta\delta$ of 0.08 ppm. The strong coordination between $-COO^-$ and Zn^{2+} reduces the electron donating ability of $-COO^-$ and hence lowers the electron cloud densities of nearby atoms. Similarly, as shown in Fig. S11 for the case of OPDP, the resonance peaks of C and H atoms close to $-SO_3^-$ also shift downfield after the introduction of $ZnSO_4$. In contrast, the $\Delta\delta$ values of OPDP are smaller than those of OCBA, verifying the stronger coordination interaction between OCBA and Zn^{2+} compared to that between OPDP and Zn^{2+}. In other words, OCBA is more capable of perturbing the local electronic environment of Zn^{2+} than OPDP. Consequently, through the formed ion-transport channels,[36] the migration of Zn^{2+} is easier in the OCBA-containing electrolyte compared to that in the OPDP-containing electrolyte.

Other spectroscopic characterization was further used to reveal the modulation mechanisms of the additives on the solvation structure of the electrolyte as well as the interactions between the ingredients. Relative to the BE, upon increasing the content of OCBA, the chemical shift of water protons exhibits an upfield shift in the ^1H NMR spectra (Fig. S12a). This observation confirms that the introduction of OCBA disrupts the hydrogen-bonding network among water molecules through the interactions between H_2O and zwitterionic groups, thereby increasing the local electron cloud density of H atoms. As shown in Fig. 2b, at the same concentration of additive (2 wt%), OPDP displays a greater impact on the hydrogen-bonding network of water than OCBA, possibly due to the larger group volume and more polar oxygen atoms on the sulfonate, which can result in a larger coordination number of H_2O.[38] Fourier transform infrared (FTIR) and Raman spectra were also acquired. As shown in the FTIR spectra (Fig. S12b), the O–H stretching
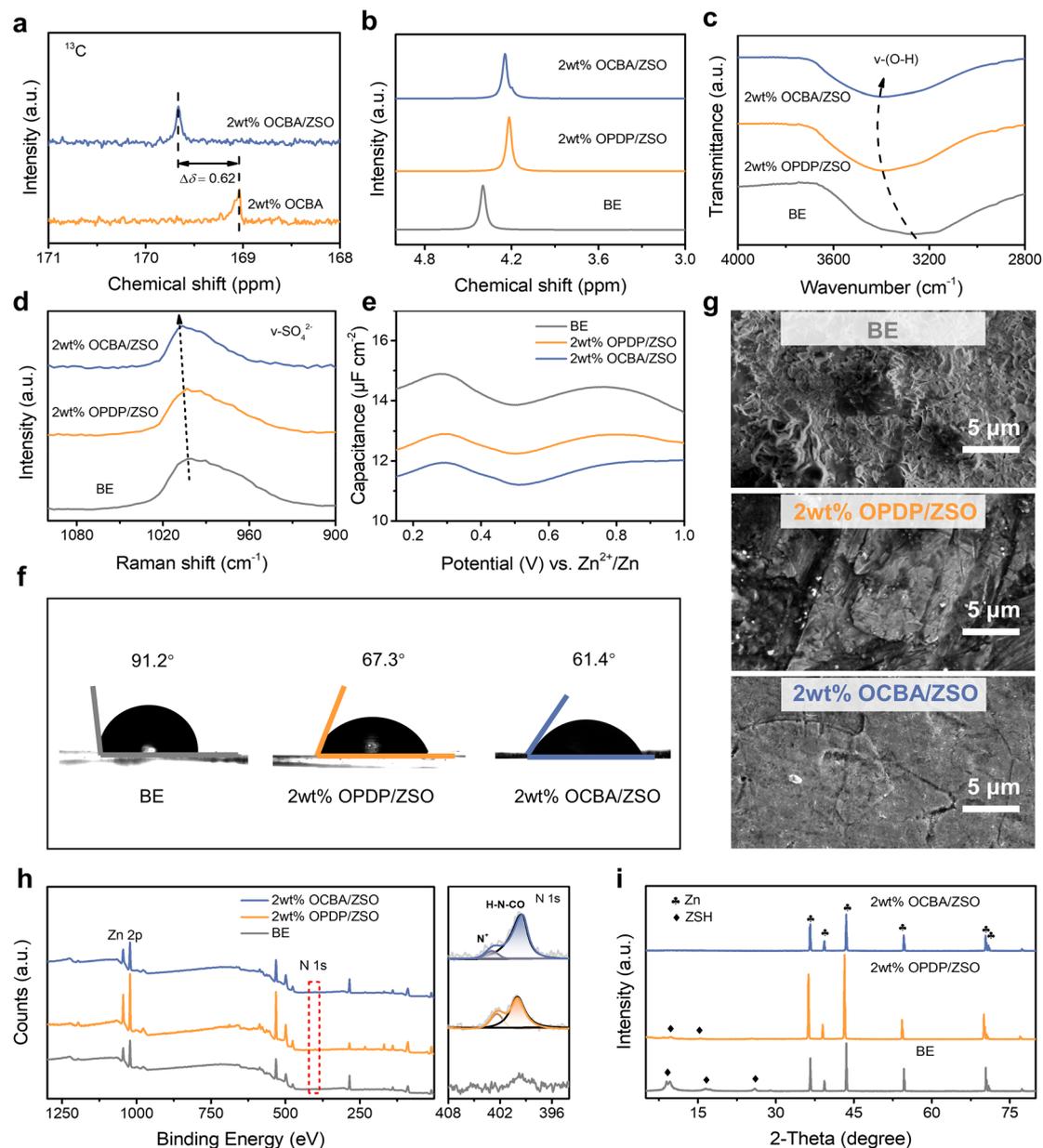
Fig. 2 Characterization of bulk electrolytes and interfaces. (a) ^{13}C NMR shifts of OCBA in water with and without the addition of ZnSO$_4$. (b) ^{1}H NMR shifts of H$_2$O in the BE, 2 wt% OPDP/ZSO, and 2 wt% OCBA/ZSO. (c) FTIR spectra of the BE, 2 wt% OPDP/ZSO, and 2 wt% OCBA/ZSO (in the OH$^-$ vibration range). (d) Raman spectra of SO$_4^{2-}$ vibration in the BE, 2 wt% OPDP/ZSO, and 2 wt% OCBA/ZSO. (e) Differential capacitance curves of Zn//Cu cells with different electrolytes. (f) Contact angles of the BE, 2 wt% OPDP/ZSO, and 2 wt% OCBA/ZSO on Zn metal. (g–i) SEM images, XPS spectra and XRD patterns of Zn metal after immersion in the BE, 2 wt% OPDP/ZSO, and 2 wt% OCBA/ZSO for 7 days. The right panel of Fig. 2h displays the deconvoluted N 1s signals.

vibration peak (ν(O–H)) blue-shifts with the increase of OCBA concentration, further verifying that OCBA weakens the strong hydrogen bonding between water molecules. The Raman spectra in Fig. S12c display the same shifting trend. Consistent with the ^{1}H NMR result, as shown in Fig. 2c, OPDP induces a more intense impact on the hydrogen bonding network of the electrolyte. Additionally, the characteristic vibrational peak of SO$_4^{2-}$ (ν(SO$_4^{2-}$)) is also considered. With the introduction of additives, the peak of ν(SO$_4^{2-}$) shifts toward higher wavenumbers (Fig. S12b and c). This reflects the ionic pair

interaction between SO$_4^{2-}$ and Zn^{2+} being weakened through the coordination of zwitterionic groups with Zn^{2+}. As discussed above, the coordination ability of OCBA with Zn^{2+} is higher than that of OPDP, which is also certified by the Raman shift in Fig. 2d.

Subsequently, the impact of additives on the electrochemical stability of the electrolytes was evaluated by linear scanning voltammetry (LSV). As shown in Fig. S13a, the onset potential of the HER (vs. Ag/AgCl) decreases from −1.014 V in the BE to −1.029 V in 2 wt% OPDP/ZSO and −1.034 V in 2 wt% OCBA/

ZSO. This indicates that both zwitterionic additives can effectively inhibit the HER in the ZnSO₄ electrolyte. Similarly, as shown in Fig. S13b, the increase in the oxygen evolution reaction (OER) potential confirms the beneficial role of zwitterionic additives in improving the electrochemical stability of water. In contrast to OPDP, OCBA exhibits more positive effects. This behavior suggests that the adsorption of OCBA on the electrode surpasses its impact on the hydrogen bond network.

The influences of zwitterionic additives on the electrode/electrolyte interfacial layer (i.e. the EDL) structure were further explored by measuring the electric double layer capacitance (EDLC) on the Zn metal surface. As shown in Fig. S14, based on cyclic voltammetry (CV) at different scan rates with a Zn//Zn cell configuration, the EDLC in the OCBA containing electrolyte is significantly lower than that in the BE or in the OPDP containing electrolyte. The adsorption of additives on the Zn surface effectively reduces the number of active sites, therefore resulting in less Zn^{2+} adsorption/desorption on the electrode during the CV process. The higher affinity of OCBA for the Zn electrode leads to a greater reduction in the number of active sites, therefore contributing to a smaller EDLC. The differential capacitance curves provide more insights into the capacitance variation and EDL structural evolution induced by different additives. In this method, the potential zero charge (PZC), defined as the electrode potential without net surface charge (corresponding to the minimum surface capacitance), serves as the indicator of EDL structure change.[15,42] The positive shifts of the PZC in Fig. 2e with the introduction of OCBA or OPDP indicate that both additives have affected the EDL structure of the Zn electrodes, while OCBA generates a more significant impact. Moreover, the addition of both zwitterionic additives significantly reduces the interfacial impedance (Fig. S15). That is, although the occupation of electrochemically active sites by OPDP or OCBA reduces the EDLC, their high hydrophilicity can lower the migration resistance of Zn^{2+} at the interface, which is very beneficial for homogeneous electric field distribution and uniform Zn deposition. Contact angle (CTA) tests were performed to verify the wettability of the three electrolytes on Zn (Fig. 2f). The CTA decreases from 91.2° for the BE to 67.3° for 2 wt% OPDP/ZSO and to an even lower value of 61.4° for 2 wt% OCBA/ZSO. This certifies that the hydrophilic –COO⁻ groups on OCBA can more effectively enhance the electrolyte affinity for the Zn metal surface and decrease the interfacial free energy, therefore facilitating the transport of Zn^{2+} across the interface.

According to previous reports, moderate additive adsorption on the electrode can be beneficial to uniform Zn deposition,[18,29] while excessive and uneven interfacial adsorption of the additive may result in interfacial current fluctuations and inhomogeneous Zn plating.[7,43] Likewise, insufficient additive adsorption fails to regulate Zn deposition, leading to severe dendrite growth during Zn plating/stripping.[29] Therefore, a quartz crystal microbalance with dissipation monitoring (QCM-D) was employed to probe the adsorption behavior of the zwitterionic additives by monitoring the frequency (Δf) and dissipation (ΔD) changes. A negative Δf shift serves as a direct indicator of the adsorption level, and a ΔD shift reveals the uniformity of the adsorbed layer. As shown in Fig. S16, a notable

negative Δf remains with the OCBA-based electrolyte after rinsing with water, indicating the effective formation of an OCBA adsorption layer. In contrast, Δf shifts are negligible for the BE and the OPDP-based electrolyte, verifying that OCBA exhibits stronger adsorption on the electrode than OPDP. Moreover, the small change of ΔD shows the homogeneous structure of the OCBA layer, which is conducive to eliminating the tip electric fields and realizing an even current distribution.

The impact of the additive adsorption layer on the corrosion resistance of the Zn electrode was subsequently evaluated by Tafel tests. As shown in Fig. S17, relative to the situation in the BE, the corrosion current density of Zn in 2 wt% OCBA/ZSO is markedly lowered to 0.194 mA cm⁻², which is also lower than that in 2 wt% OPDP/ZSO (0.237 mA cm⁻²), indicating that OCBA effectively suppresses Zn corrosion. Additionally, the increased corrosion potential further confirms the effective protection of the OCBA layer against Zn self-corrosion. Furthermore, after soaking polished Zn foils in BE, 2 wt% OCBA/ZSO, and 2 wt% OPDP/ZSO for 7 days, the surface morphologies were compared by scanning electron microscopy (SEM). As shown in Fig. 2g and S18, severe corrosion and irregular protrusions on the Zn foil are observed after the treatment with the BE. In contrast, the Zn foil treated with 2 wt% OCBA/ZSO exhibits a smooth and dense morphology, while that treated with 2 wt% OPDP/ZSO still shows slight dendrite formation. Confocal laser scanning microscopy (CLSM) was further adopted to characterize the surface morphology evolution of Zn foils within different electrolytes (Fig. S19). After soaking in the BE, the Zn surface shows a notably rough structure, and that in 2 wt% OPDP/ZSO also exhibits an inhomogeneous morphology with protrusions. Remarkably, the Zn surface from 2 wt% OCBA/ZSO achieves a smooth and homogeneous deposition morphology. Protrusions and dendrites on the Zn surface will cause localized electric field intensification and induce further corrosion, which is extremely harmful to the anode stability during the calendar-aging period.

The adsorption of the additive on Zn foil after soaking treatment was also verified by elemental analysis. An abundant and uniform distribution of N on the Zn foil in 2 wt% OCBA/ZSO was observed using energy dispersive spectroscopy (Fig. S18f). As further displayed in Fig. 2h, X-ray photoelectron spectroscopy (XPS) analysis shows that an obviously richer N 1s signal appears on that Zn surface compared to those in the other two electrolytes, confirming the effectively formed OCBA protective layer on the surface of Zn during the immersion process. It should be noted that the weak N 1s signal in the BE sample should originate from the background noise or trace contamination during the XPS measurement. As inferred, a uniform adsorption layer of OCBA in the EDL effectively blocks the direct contact between water molecules and the Zn metal, thereby suppressing side reactions. Then, X-ray diffraction (XRD) measurements were used to identify byproducts formed on the Zn surfaces after soaking in different electrolytes (Fig. 2i). The characteristic diffraction peaks of $Zn_4(OH)_6SO_4$·$3H_2O$ (ZSH) are detected on the Zn surfaces in the BE and 2 wt% OPDP/ZSO, whereas no such peaks are observed for 2 wt% OCBA/ZSO.

Effects of additives on the Zn deposition behavior

The effects of zwitterionic additives on the behavior of Zn^{2+} were then compared, including migration in solution, transference across the electrolyte–electrode interface, and deposition on the electrode. The transference numbers of Zn^{2+} ($t_{Zn^{2+}}$) in different electrolytes were determined according to the Evans method. As shown in Fig. S20, $t_{Zn^{2+}}$ is remarkably improved after the introduction of either zwitterionic additives, and OCBA is more effective than OPDP. The strong interactions between OCBA and the ions are helpful in breaking the ion-pair effects between Zn^{2+} and SO_4^{2-}, which thereby increases $t_{Zn^{2+}}$ effectively. That is, although the conductivity of the electrolyte slightly decreases with the introduction of OCBA, the migration of Zn^{2+} is largely facilitated;[29] consequently, the cation depletion and polarization near the electrode can be well relieved. Desolvation occurring near the OHP is an essential prerequisite for the entrance into the IHP of Zn^{2+} to receive electrons. Therefore, E_a in different electrolytes was subsequently evaluated. After carrying out electrochemical impedance spectroscopy (EIS) at various temperatures (Fig. S21), the charge transfer resistance (R_{ct}) at different temperatures was measured, and E_a was determined based on Arrhenius equation fitting (Fig. S22). As calculated, E_a values in the electrolytes with OCBA and OPDP additives are 15.3 and 16.9 kJ mol^{-1}, respectively, which are much smaller than that in the BE (25.3 kJ mol^{-1}). The reduction in the desolvation energy barrier of Zn^{2+} facilitates the Zn deposition/exfoliation kinetic process.[18] Overall, as shown in Fig. 3a, compared to previously reported electrolytes based on other zwitterionic additives, due to the all-round regulation of OCBA, the electrolyte demonstrates a well-balanced enhancement in various electrochemical properties.[28,44–46]

To further verify whether the EDL structure modified by the additive adsorption layer facilitates the deposition of Zn, the nucleation and deposition behaviors of Zn^{2+} were investigated. First, the initial nucleation behaviors of Zn in different electrolytes were compared using the CV method in Zn//Cu cells. As shown in Fig. S23, the introduction of OPDP and OCBA increases the nucleation overpotential (η) by 18 and 33 mV, respectively. According to the Gibbs free energy minimization principle and the classical nucleation theory, a higher η enhances the nucleation driving force, promoting the formation of smaller and more uniformly distributed Zn crystalline grains, thereby favoring denser Zn deposition.[47] Thereby, the stronger affinity of OCBA with the Zn metal compared to that of OPDP results in a greater effect. Subsequently, chronoamperometry (CA) measurements were conducted to analyze the growth mechanisms of Zn deposition during plating. As displayed in Fig. S24, under a fixed overpotential of −150 mV, the current density in the BE continuously increases over 400 s, indicating long-term two-dimensional (2D) diffusion of Zn^{2+} on the surface (*i.e.* the vertical growth of Zn dendrites). The clear current density also suggests very uneven Zn deposition in the BE. In contrast, in electrolytes with zwitterionic additives, the 2D diffusion is almost stabilized within 30 s, indicating that the additive adsorption layer on the Zn surface significantly inhibits Zn^{2+} horizontal diffusion, thus enhancing the uniformity of

nucleation and deposition. In comparison with OPDP, the stronger interactions between OCBA and Zn/Zn^{2+} realize better control of the Zn deposition behavior and kinetics, and hence a much lower and more steady current density is exhibited. This also contributes to the enhanced nucleation driving force (Fig. S23) and promotes smaller and more uniformly distributed Zn crystalline grains.

The evolution of the electrolyte–electrode interface during deposition/stripping cycling was then evaluated by an *in situ* EIS investigation (Fig. 3b–d and S25). With the BE, the R_{ct} exhibits a continuous downward trend; this implies that progressive interfacial degradation (including uneven Zn deposition and ZSH byproduct formation) is induced by the electrolyte. In comparison, the addition of OCBA stabilizes the R_{ct} from the first cycle, verifying the high stability of the electrode interface under the protection of the OCBA adsorption layer. In the case of OPDP, due to its insufficient protection, small fluctuations of R_{ct} are exhibited with a much higher average R_{ct} value compared to that with OCBA, suggesting a relatively high ionic transfer resistance and slightly unstable electrode interface. The Zn surfaces after cycling in different electrolytes were further analyzed by SEM and XRD. As shown in Fig. S26a, after 30 cycles in the BE, the Zn electrode surface becomes loose and is full of irregular protrusions. Upon continuing to 60 cycles, the deposited layer shows a highly disordered structure covered with lamellated dendrites. This undesired morphology evolution critically impairs the reversibility of the Zn anode and emerges as the primary failure mechanism of the battery. A similar trend is observed on the Zn anode with 2 wt% OPDP/ZSO, while this unfavorable situation is much less serious (Fig. S26b). The XRD results in Fig. 3e show obvious byproduct peaks related to ZSH at ~8° on the Zn anode after 60 cycles within the BE or 2 wt% OPDP/ZSO, indicating that the as-observed disordered lamellas contain abundant inactive byproducts. Impressively, after 30 cycles within the OCBA-based electrolyte, the deposited Zn layer exhibits a dense and homogeneous morphology without any visible dendrites (Fig. S26c). This morphology is well maintained after 60 cycles. The slight ratio changes from 30 to 60 cycles indicate that the preferential deposition orientation of Zn is mainly established at the very early stage of cycling, so that crystal plane reconstruction during prolonged cycling is not significant. This further demonstrates the superior ability of OCBA in guiding the Zn deposition. The XRD patterns in Fig. 3e also exclude the existence of ZSH byproducts in this situation. Moreover, the XRD patterns display different preferred Zn crystal planes for Zn anodes after cycling in the three electrolytes. By comparing the relative peak intensities of (002) and (101) of Zn ($I_{002} : I_{101}$), it is concluded that OCBA can more effectively guide the Zn deposition along the Zn (002) plane. This tendency assists compact Zn deposition, and also suppresses side reactions and dendrite formation during long-term cycling. CLSM further confirms the regulated deposition of the Zn anode after 60 cycles in 2 wt% OCBA/ZSO compared to the other two electrolytes (Fig. S27). With the BE, the Zn surface shows particularly rough features with large protrusions of about 23.7 μm in height; the Zn foil after cycling in 2 wt% OPDP/ZSO shows an inhomogeneous distribution of
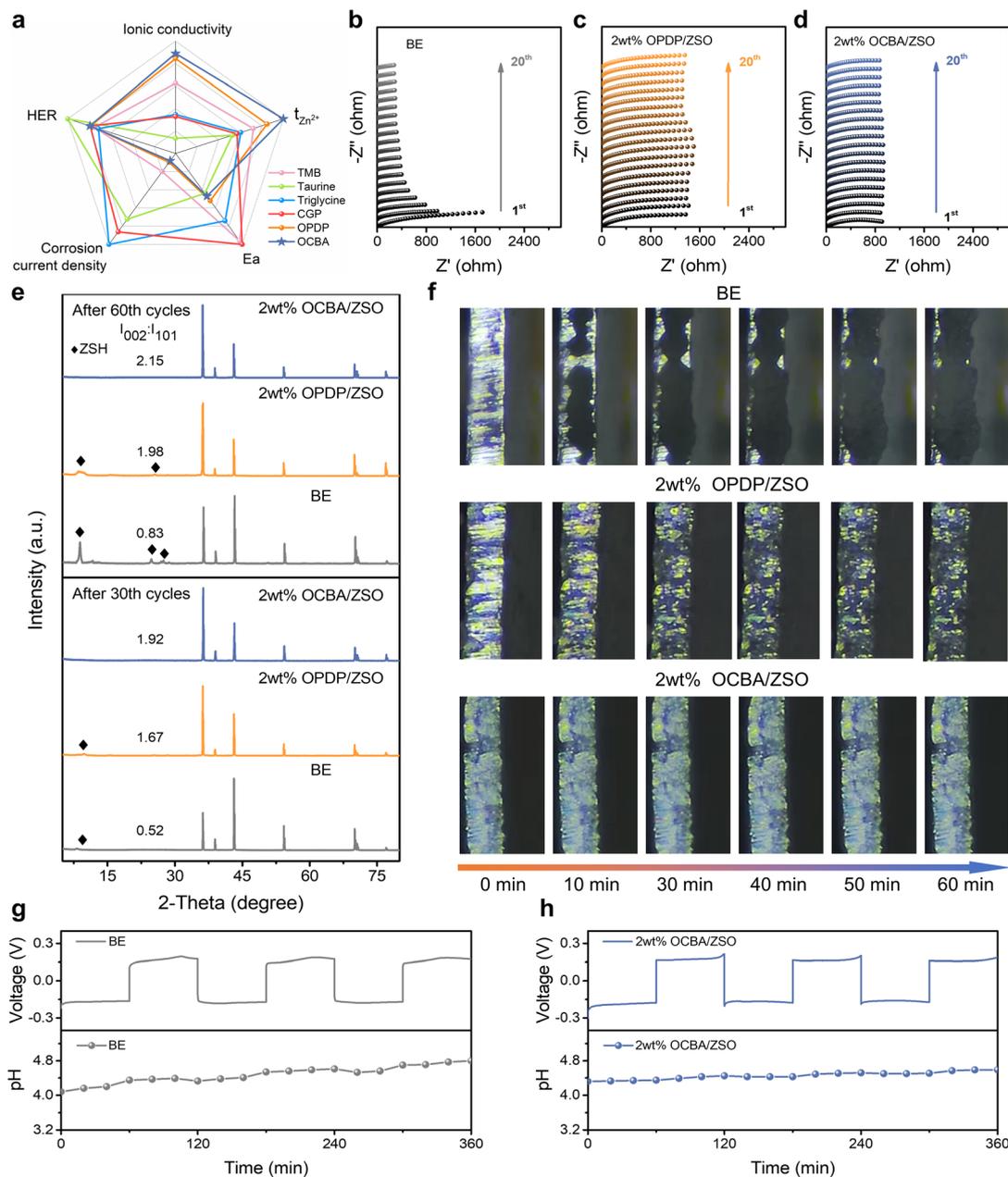
Fig. 3 The effect of additives on the interfacial behavior of the Zn anode. (a) A comparison of the performance of 2 wt% OCBA/ZSO with previously reported electrolytes based on other zwitterionic additives. *In situ* EIS curves of Zn//Zn batteries with (b) the BE, (c) 2 wt% OPDP/ZSO, and (d) 2 wt% OCBA/ZSO. (e) XRD patterns of Zn metal after cycling for 30 cycles and 60 cycles in different electrolytes. (f) Time-dependent optical microscopy images showing Zn plating behavior in different electrolytes. Time-voltage curve and real-time pH evolution near the Zn anode in (g) the BE and (h) 2 wt% OCBA/ZSO during the plating/stripping process.

dotted Zn deposition. In contrast, the Zn anode surface after cycling in 2 wt% OCBA/ZSO is free of dendrites and protrusions. Furthermore, as shown in Fig. S28, the CTA on the Zn anode notably decreases after cycling in the BE or 2 wt% OPDP/ZSO (the hydrophilic byproducts and the roughness on the anode interfaces both contribute to the reduction of the CTA). Nevertheless, the CTA on the Zn anode cycled in the OCBA-based electrolyte almost remains unchanged (compared to that in Fig. 2f); this is highly consistent with the EIS results in Fig. 3d. Additionally, the higher CTA of the OCBA-based electrolyte on

the anode can help to hinder water penetration, therefore further reducing the side reactions of the electrode.

The regulation effect of additives on the Zn plating dynamics can be better visualized by an *in situ* optical microscopy investigation. As shown in Fig. 3f, under a constant current density of 1 mA cm^{-2}, the Zn anode in the BE experiences a rapid formation of uneven and bulky deposits, as demonstrated by the tarnished Zn surface after only 10 minutes of plating. In the OPDP-based electrolyte, the nonuniform deposition is partially mitigated. With the addition of OCBA, the shiny metallic luster

of the Zn foil is well retained. That is, in this case, the Zn nucleation process becomes markedly uniform, and the deposition layer remains dense with fine grains. Moreover, no hydrogen evolution bubbles are observed throughout the whole electroplating process with OCBA. These results demonstrate that OCBA effectively regulates Zn^{2+} deposition behavior and suppresses side reactions such as hydrogen evolution and byproduct formation, thereby significantly enhancing the stability and reversibility of Zn anode deposition.

It is also worth noting that Zn deposition can be strongly influenced by pH fluctuations. The abundant ZSH byproduct in the BE, as displayed in Fig. 3e, originates from the HER during cycling, which suggests that the local concentration of OH^- should experience a progressive increase. In order to prove this,

a simple symmetric cell configuration was constructed for *in situ* pH monitoring during plating/stripping cycling (Fig. S29a). As shown in Fig. 3g, after 3 cycles (360 minutes), the pH of the BE increases by 0.72 (from 4.08 to 4.80), which hints at the occurrence of severe HER. The addition of OPDP alleviates this side reaction to a certain degree, showing a reduced pH increase of 0.54 (from 4.18 to 4.72; Fig. S29b). As expected, the pH fluctuations are almost negligible in 2 wt% OCBA/ZSO, demonstrating the excellent pH buffering ability of OCBA (Fig. 3h). On the one hand, the enhanced pH after adding OCBA reduces proton activity and suppresses proton involving reactions. On the other hand, the adsorption of OCBA on the EDL diminishes the reduction reaction of water by blocking the contact between water and the Zn surface.
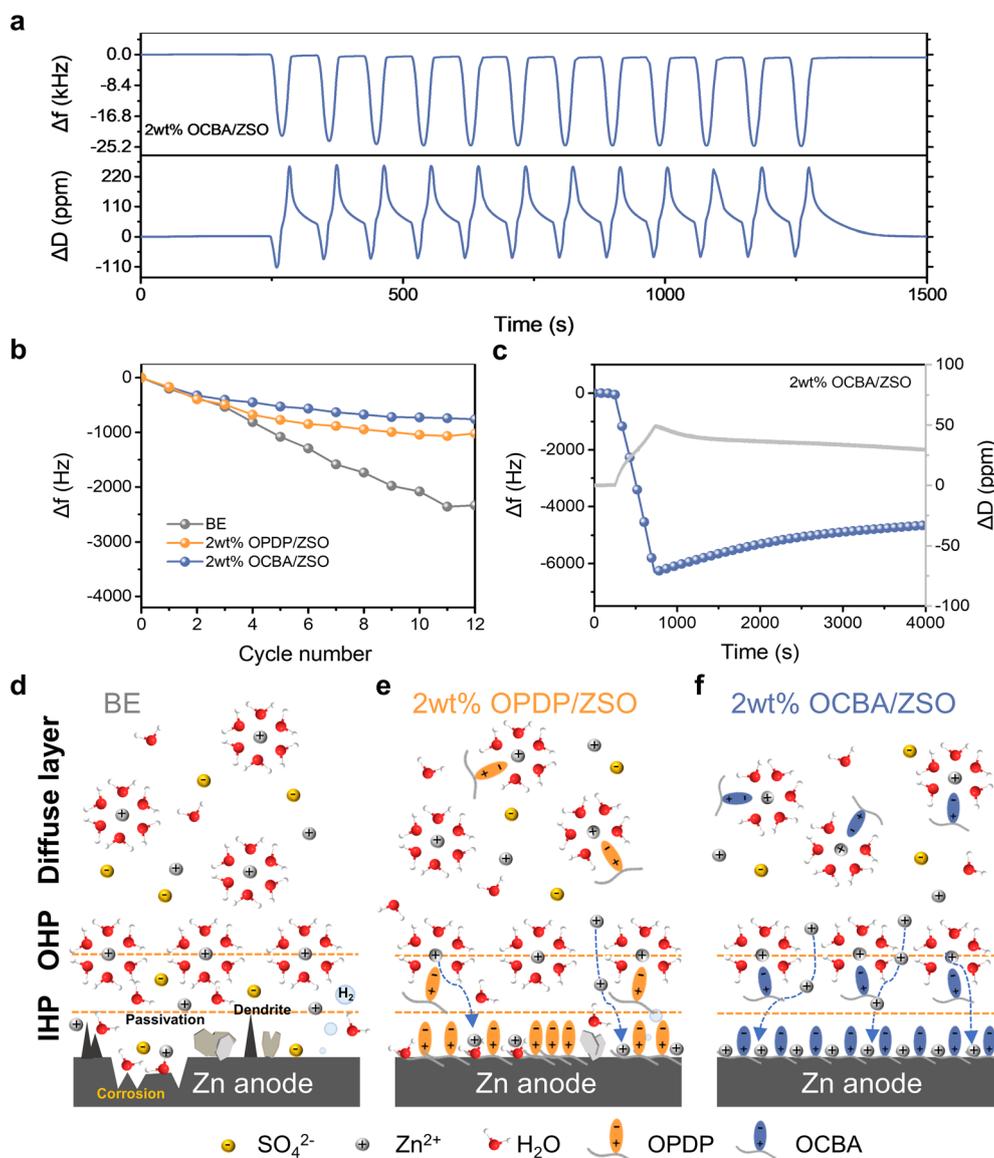

Fig. 4 Effect of additives on Zn deposition. (a) EQCM-D frequency (Δf) and dissipation (ΔD) shifts during 12 CV cycles in 2 wt% OCBA/ZSO. (b) Δf shifts during CV cycling in different electrolytes. (c) Δf and ΔD shifts during deposition at a current density of 0.5 mA cm^{-2} for 8 min and subsequent rinsing in 2 wt% OCBA/ZSO. (d–f) A schematic illustration of the composition-related electrolyte structures and interfacial electrochemical processes for the BE, 2 wt% OPDP, and 2 wt% OCBA electrolytes.

Essentially, additives should be effective in boosting the battery cycling kinetics and lifespan. The cycling performance of the electrode in different electrolytes was further explored with an electrochemical EQCM (EQCM-D) by applying a CV procedure. The real-time Δf and ΔD shifts of the QCM-D with great accuracy can provide mass and structure variation information during plating and stripping. As shown in Fig. 4a and b, with 2 wt% OCBA/ZSO, excellent cycling stability is demonstrated by the subtle shifts in Δf after each CV cycle. A total negative Δf shift of ≈ 760 Hz is only achieved after 12 CV cycles. Simultaneously, ΔD returned to 0 after the CV procedure was finished; that is, the OCBA additive promotes homogeneous Zn deposition, and the deposited Zn is completely exfoliated in the subsequent stripping procedure. The slight residual Δf might result from the dense SEI structure assisted by the reduction of OCBA.[29] When using the BE (Fig. S30a and b), the Δf decreases rapidly as the CV cycling progresses, leading to a total negative Δf change of 2340 Hz and a ΔD change of 11.5 ppm after 12 cycles. The residual Δf and ΔD should be caused by the ZSH byproduct and "dead" Zn from the loose dendrites, suggesting the inhomogeneous deposition of the Zn layer and the poor cycling reversibility of the Zn anode. As indicated in Fig. 4b, S30c and d, OPDP also shows the ability to improve Zn anodic reversibility by regulating Zn^{2+} deposition and reducing side reactions, but its effectiveness is much weaker than that of OCBA.

Subsequently, the galvanostatic method was adopted for EQCM-D measurements to explore the Zn^{2+} deposition dynamics. As shown in Fig. S31a, during an 8 min plating in the BE at a current density of 0.5 mA cm^{-2}, the rapid decrease in Δf indicates the occurrence of Zn deposition, but the deposition rate is nonlinear and highly unsteady. At the same time, ΔD increases to over 400 ppm, revealing a very rough and porous deposition structure with the formation of dendrites as well as disarrayed ZSH sheets. After the current input ceases, the following decline in Δf and the increase in ΔD imply the continuous growth of ZSH. As shown in Fig. 4c with 2 wt% OCBA/ZSO, the linear change in Δf during the plating process demonstrates steady and homogeneous deposition kinetics. The resultant small ΔD shift indicates uniform and compact Zn deposition without dendrite formation; compared to those for 2 wt% OPDP/ZSO (Fig. S31b), the smaller Δf but larger ΔD during plating should result from the elimination of ZSH formation and the co-adsorption of OCBA during plating. Besides, within the calendar-aging process in the OPDP-based electrolyte (Fig. S31b), a continuous increase in ΔD is observed, which should result from the growing porosity induced by the partial dissolution of the deposited Zn layer (from which "dead" Zn is produced within the following stripping process). No such phenomenon is observed for OCBA in Fig. 4c, further verifying that the co-adsorbed OCBA effectively protects the deposited Zn layer from dissolution during shelving.

The mechanism for how the OCBA modulates highly reversible Zn plating/stripping is illustrated in Fig. 4d–f. In summary, aiming at synergistically strengthening the interactions between additives and $H_2O/Zn^{2+}/Zn$ metal, OCBA shows a comprehensive capability to modulate all relevant aspects from the electrolyte bulk phase to the EDL; consequently, Zn nucleation and deposition behaviors are well regulated while dense deposition is fully achieved (Fig. 4f).

Effects of additives on the electrochemical performance of batteries

Zn//Cu asymmetric cells with different electrolytes were first assembled to evaluate their influence on the CE during battery cycling. As shown in Fig. 5a, the Zn//Cu cell with the BE fails rapidly at 1 mA cm^{-2} and 1 mAh cm^{-2}, mainly due to the fast-growing dendrites. The low CE displayed in Fig. 5b suggests severe side reactions. In contrast, with the comprehensive modulation of OCBA from the bulk electrolyte to the electrode–electrolyte interface, side reactions are effectively inhibited and uniform Zn deposition is promoted, significantly improving the plating/stripping lifespan to ≈ 3000 cycles (5980 h) with an average CE of 99.7%. The OPDP additive also realizes a degree of enhancement in the lifespan, but the CE of the cell starts to fluctuate after around 900 cycles, which is mainly attributed to localized dendrite aggregation. Furthermore, the initial CE values of the Zn//Cu cells at different current densities (0.25–5 mA cm^{-2}) are compared (Fig. S32). The BE-based cells exhibit the lowest initial CE over all current densities, implying pronounced parasitic reactions. The cells with 2 wt% OPDP/ZSO achieve a certain enhancement of the CE, confirming that the OPDP additive possesses the capacity to inhibit side reactions. Impressively, the cells with 2 wt% OCBA/ZSO deliver highly favorable initial CE values at all tested current densities, reaching up to 98% at 5 mA cm^{-2} and 5 mAh cm^{-2}. An average CE (CE$_{avg}$) method was adopted to reflect the initial loss of active Zn in the earlier cycling stage (Fig. S33). In the BE, a CE$_{avg}$ of 91.3% is exhibited, indicating a significant irreversibility due to side reactions and interfacial instability of the Zn anode. In comparison, the OPDP-based electrolyte results in an improved CE$_{avg}$ of 97.5%, and strikingly, the cell with the OCBA additive delivers a highly stable voltage profile with a CE$_{avg}$ of 98.1%, confirming that OCBA can significantly enhance the interfacial stability and reversibility of Zn^{2+} plating/stripping by effectively suppressing side reactions. This improved performance as a result of OCBA is attributed to the strong coordination of carboxyl groups with Zn^{2+} as well as the interactions between carboxyl groups and the Zn metal, which effectively enhance the Zn utilization efficiency during the plating process. On the other hand, as demonstrated in Fig. S34, the adsorption of OCBA on the Zn anode displays dynamic behaviors, where partial desorption occurs during the stripping process; this dynamic behavior of OCBA guarantees high cycling reversibility and a high CE when stripping.[29,32]

The rate capabilities of symmetric Zn//Zn cells were subsequently evaluated (Fig. S35). The cell with the BE exhibits rapid short-circuiting at a capacity of 10 mAh cm^{-2}, indicating poor stability under high-rate conditions due to severe dendrite growth. The Zn//Zn cell with 2 wt% OPDP/ZSO shows an improved rate performance, but its long-term cycling stability is still limited at a high rate. Notably, the cell employing 2 wt%
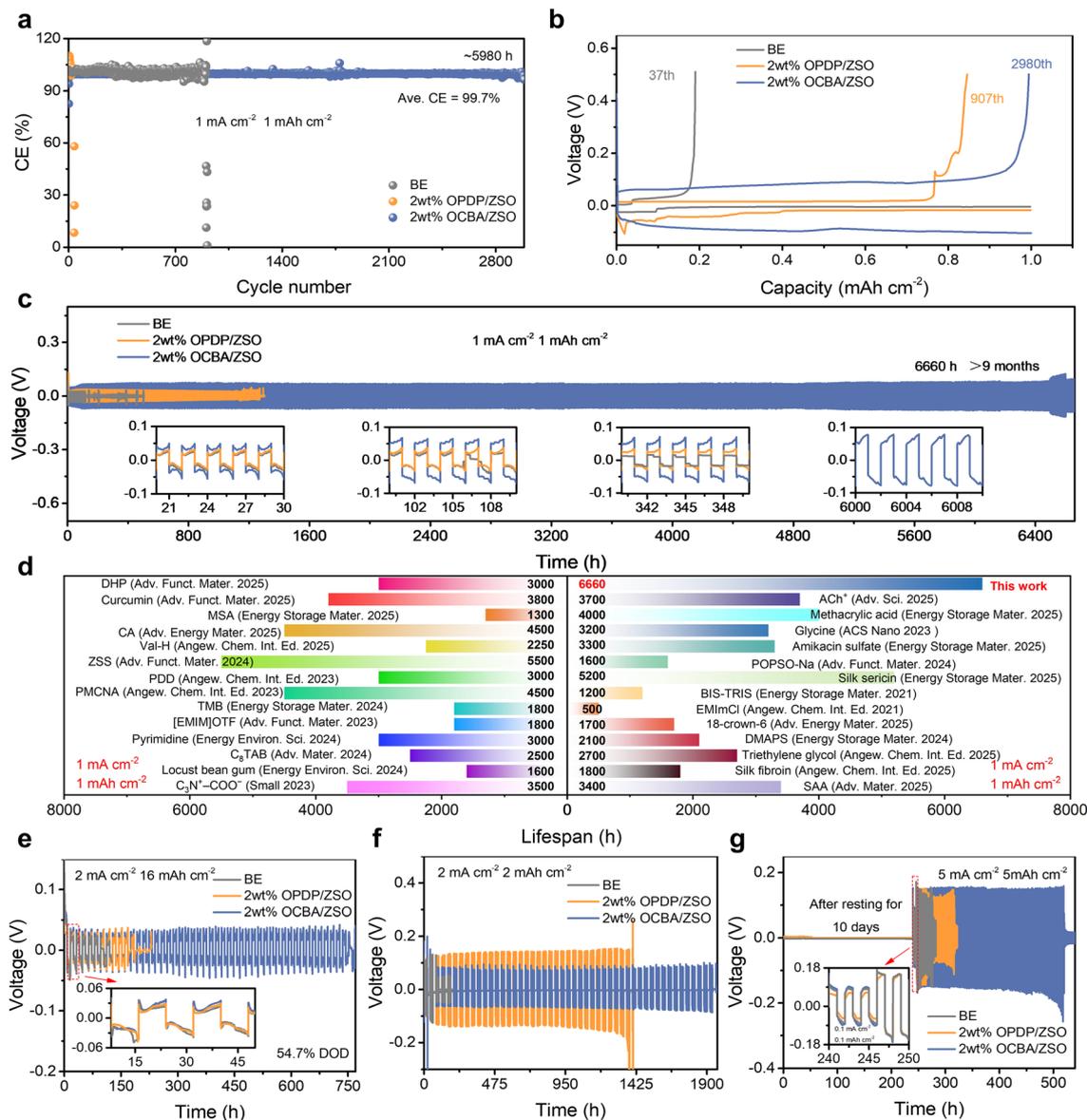
Fig. 5 Effects of additives on the electrochemical performance of Zn anodes. (a) CE comparison of Zn//Cu cells in the BE, 2 wt% OPDP/ZSO, and 2 wt% OCBA/ZSO at 1 mA cm^{-2} and 1 mAh cm^{-2}. (b) Corresponding voltage profiles at different cycle numbers from (a). (c) Cycling performance of Zn//Zn batteries with different electrolytes at 1 mA cm^{-2} and 1 mAh cm^{-2}. (d) A comparison of the cycling stability of Zn symmetric cells with previous reports at 1 mA cm^{-2} and 1 mAh cm^{-2}. (e) Cycling performance of Zn//Zn symmetric cells with different electrolytes at 2 mA cm^{-2} and 16 mAh cm^{-2} under a DOD of 54.7%. (f) Shelving-recovery performance of Zn//Zn symmetric cells with the BE, 2 wt% OPDP/ZSO, and 2 wt% OCBA/ZSO at 2 mA cm^{-2} and 2 mAh cm^{-2}. (g) Cycling performance of Zn//Zn cells with the BE, 2 wt% OPDP/ZSO, and 2 wt% OCBA/ZSO after resting for 10 days.

OCBA/ZSO exhibits excellent reversibility over the entire range of current densities, underscoring the superior electrochemical stability. By effectively suppressing side reactions and promoting uniform and dense zinc deposition with OCBA, the reversibility and interfacial stability during plating/stripping cycling are effectively enhanced for realizing prolonged lifespans at different current densities. Long-term cycling tests of Zn//Zn symmetric cells were conducted at 1 mA cm^{-2} and 1 mAh cm^{-2} (Fig. 5c). The cell using the BE suffers from severe side reactions and dendrite growth, leading to short-circuiting after only 29 h of cycling. The cell with the OPDP-based

electrolyte also shows a limited lifespan of 1100 h due to the insufficient regulation ability of OPDP. Notably, the electrolyte containing 2 wt% OCBA endows the cell with outstanding stability, achieving a remarkable cycling lifespan of over 6660 h (>9 months) with consistently stable polarization voltage, outperforming most previously reported Zn//Zn batteries (Fig. 5d and Table S1). The higher polarization voltage using 2 wt% OCBA/ZSO is attributed to the enlarged nucleation overpotential compared to those using the other two electrolytes (Fig. 5b and S23). This is helpful in forming smaller and more

uniformly distributed Zn crystalline grains, further facilitating the extended cycling lifespan of the batteries.

Meanwhile, the ability to inhibit gas evolution reactions during battery cycling was evaluated for the different electrolytes, by comparing the thickness variations of the corresponding Zn//Zn symmetric cells at different cycling stages. As shown in Fig. S36, the cell thickness using the BE progressively increases by 0.67 mm in 200 cycles, reflecting severe cell swelling by gas accumulation. When using 2 wt% OPDP/ZSO, the change of the cell thickness slows down, increasing by 0.23 mm in 200 cycles. Notably, the thickening phenomenon is minimal for the cell with 2 wt% OCBA/ZSO, with the thickness only increasing by 0.13 mm in 200 cycles; in particular, the thickness of this cell almost remains constant after the first 10 cycles, which demonstrates the significant advantages of OCBA in stabilizing the interface and inhibiting the side-reactions (especially gas generation). Furthermore, the battery performance with different electrolytes under a high depth of discharge (DOD) of 54.7% (2 mA cm^{-2} and 16 mAh cm^{-2}) is compared (Fig. 5e). The Zn//Zn cell with 2 wt% OCBA/ZSO exhibits a prolonged cycling lifespan exceeding 750 h, whereas the cells based on the BE and 2 wt% OPDP/ZSO fail after 94 and 171 h, respectively. This indicates that the introduction of OCBA effectively suppresses parasitic reactions and dendrite growth even under severe conditions of ultra-high zinc utilization.

In practice, batteries are less likely to be charged/discharged ceaselessly; therefore, resting-recovery tests are necessary to assess the practical stability of the electrode in selected electrolytes. As shown in Fig. 5f, under intermittent operation, Zn//Zn cells were cycled for 10 cycles at 2 mA cm^{-2} and 2 mAh cm^{-2}, followed by resting for 20 h. Remarkably, the OCBA-based battery maintains stable operation for over 1900 h, while the BE and 2 wt% OPDP/ZSO based batteries only sustain stable operation for 171 and 1420 h, respectively. Even at a higher current density of 5 mA cm^{-2} and a capacity density of 5 mAh cm^{-2}, the OCBA-containing electrolyte still enables the cell to work stably for over 390 h, far better than the other two types of electrolytes (Fig. S37). Additionally, as shown in Fig. 5g, Zn//Zn batteries were initially rested for 10 days and were then evaluated for cycling stability. Cells with the BE and 2 wt% OPDP/ZSO both experience rapid short-circuit failures, while the cell using 2 wt% OCBA/ZSO sustains steady operation for ≈ 300 h, suggesting that the OCBA additive effectively enhances battery lifespan and safety for practical usage.

Finally, PANI cathodes were used to construct Zn//PANI full batteries with different electrolytes to further verify the feasibility of the OCBA additive. As shown in Fig. 6a, the Zn//PANI batteries using BE, 2 wt% OPDP/ZSO, and 2 wt% OCBA/ZSO all exhibit similar CV curves, suggesting that the redox mechanism between Zn and PANI remains consistent for all three electrolytes. The Nyquist plots (Fig. S38) reveal the smallest semicircle in the high-frequency region for the battery with 2 wt% OCBA/ZSO, corresponding to reduced charge transfer resistance and thus enhanced Zn plating/stripping kinetics. Benefiting from the regulation capability of OCBA, the Zn//PANI full battery delivers an excellent cycling stability at a current

density of 1 A g^{-1}, exhibiting a high-capacity retention of 86% after 2000 cycles (Fig. 6b). In contrast, the cell using the BE undergoes short circuiting at the 440th cycle. The Zn anode morphology after 100 cycles was then characterized by SEM. As shown in Fig. S39, the Zn surface cycled in the OCBA-containing electrolyte remains smooth and compact without any dendritic formation or ZSH sheets, whereas the BE and OPDP-based electrolytes result in significant dendrite formation and protrusions.

The effects of different electrolytes for resisting self-discharge in Zn//PANI batteries were evaluated, which provides more information on how side reactions occurring inside the batteries impact their energy storage during shelving. The batteries were fully charged to 1.5 V, then rested for 24 h at their open circuit voltages, and were eventually discharged to 0.5 V to evaluate the capacity retention rate. The capacity retention of the BE-based battery is only $\approx 75\%$ (Fig. 6c), and is increased to 83% by the OPDP-based electrolyte (Fig. 6d). By using 2 wt% OCBA/ZSO, the capacity retention is further elevated to 96.2% (Fig. 6e), verifying minimal side reactions and therefore the lowest self-discharge loss. With the presence of OCBA, the water activity has been reduced to some extent. More importantly, compared to the BE or OPDP-containing electrolyte, the adsorbed OCBA layer on the Zn anode effectively inhibits hydrogen evolution and Zn self-corrosion (Fig. 4c and S31), therefore significantly slowing down the self-discharge behavior of the batteries. Moreover, the Zn//PANI full battery with the OCBA-containing electrolyte exhibits an outstanding rate performance over a wide range of current densities (0.1–3.0 A g^{-1}), clearly outperforming the other two electrolytes (Fig. 6f and S40). In particular, under high-rate conditions, the charge–discharge voltage plateaus are still well presented in the battery with the OCBA-based electrolyte (Fig. S40c), verifying good redox dynamics. It should be noted that at the early stage of rate performance tests, the battery capacity in 2 wt% OPDP/ZSO is slightly higher than that in 2 wt% OCBA/ZSO at 0.1 A g^{-1}, and a similar result can be found in Fig. 6b. A possible reason might be that OCBA can also adsorb onto the PANI surface, which makes the active materials on the cathode side less accessible.

A long-term cycling test at 3 A g^{-1} was conducted to assess the high-rate durability of the OCBA-based full batteries (Fig. 6g). After 2000 cycles, the battery retains a discharge capacity of 87.4 mAh g^{-1} (representing a capacity retention of 74.5%), indicating stable Zn plating/stripping and efficient Zn^{2+} intercalation in the PANI cathode under high current densities. A hybrid capacitor employing activated carbon as the cathode also displays excellent cycling stability, highlighting the broad applicability and versatility of the OCBA-based electrolyte in a variety of zinc ion energy storage devices (Fig. S41). Furthermore, as shown in Fig. 6h, a Zn//PANI pouch cell with 2 wt% OCBA/ZSO shows good cycling stability at 0.5 A g^{-1}, maintaining 78% of its initial capacity after 150 cycles (corresponding to energy and power densities of 112.54 Wh kg^{-1} and 134.29 W kg^{-1}). As shown in Table S2, the electrochemical performance of our Zn//PANI battery is comparable to or even better than those in previous reports. Three such pouch batteries connected
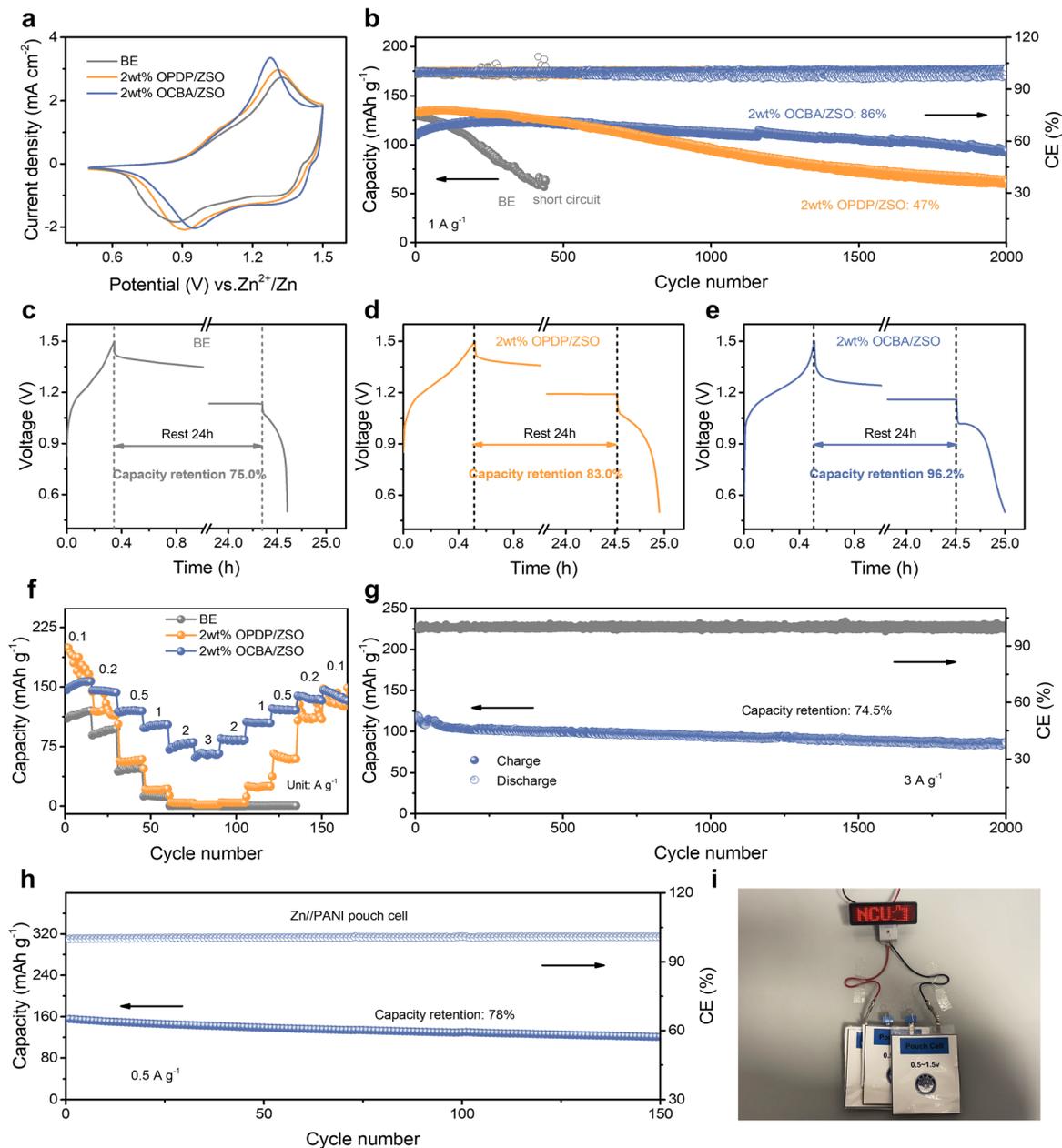
Fig. 6 Effects of additives on the electrochemical performance of Zn//PANI full batteries. (a) CV plots for 0.5 mV s^{-1} Zn//PANI cells with the BE, 2 wt% OPDP/ZSO, and 2 wt% OCBA/ZSO. (b) Cycling performance at a current density of 1 A g^{-1} of full cells with the BE, 2 wt% OPDP/ZSO, and 2 wt% OCBA/ZSO. Self-discharge curves of full cells with (c) BE, (d) 2 wt% OPDP/ZSO, and (e) 2 wt% OCBA/ZSO. (f) Rate performance of Zn//PANI batteries with the BE, 2 wt% OPDP/ZSO, and 2 wt% OCBA/ZSO. (g) Cycling performance at a current density of 3 A g^{-1} for Zn//PANI batteries with 2 wt% OCBA/ZSO. (h) Cycling stability of Zn//PANI pouch cells with 2 wt% OCBA/ZSO at a current density of 0.5 A g^{-1}. (i) Optical image of an LED panel powered by three series-linked Zn//PANI pouch batteries.

in series successfully power an LED panel (Fig. 6i), demonstrating the strong potential of this electrolyte design.

Conclusions

In summary, through the combination of theoretical calculations and experimental investigations, two zwitterionic electrolyte additives, OPDP and OCBA, are compared to reveal the significance of the comprehensive regulation of additives, from the bulk electrolyte to the interface, for high performance

AZIBs. Compared to OPDP with the sulfobetaine group, the carboxybetaine additive of OCBA with carboxylate side groups ($-COO^-$) exhibits a more multifaceted effect, including modulating the hydrogen bonding network of the electrolyte, modifying the hydration of Zn^{2+} and reducing the dehydration energy barrier, facilitating the migration of Zn^{2+} within the bulk and across the interface, re-constructing the EDL structure of the electrode, and guiding Zn deposition along the (002)-facet. As a benefit of these synergistic regulations, the HER, Zn corrosion, ZSH formation, Zn dendrite growth, and other undesired

side reactions are effectively inhibited. As a result, Zn//Zn symmetric cells exhibit a remarkably extended cycling lifespan exceeding 6660 h at 1 mA cm^{-2} and 1 mAh cm^{-2}, while Zn//Cu half-cells maintain a high CE of over 99.7% during ≈ 3000 cycles of plating/stripping. Additionally, Zn//PANI full batteries assembled with the OCBA/ZSO electrolyte demonstrate excellent rate capability and long-term cycling stability. This work emphasizes critical guidelines for the electrochemical mechanisms of electrolyte additives and provides new perspectives for developing high-performance AZIBs by additive design.

Author contributions

Y. D. carried out example synthesis, characterization, and data analysis. S. X. synthesized monomers and polymers. Z. P. commented on and revised the manuscript. L. F. conceived the idea and co-wrote the paper. T. W. conceived the idea, experimentally realized the study, supervised the project, and co-wrote the paper. All the authors took part in discussion of the results.

Conflicts of interest

There are no conflicts to declare.

Data availability

The data supporting this article have been included as part of the supplementary information (SI). Supplementary information is available: detailed experimental section, supplementary characterization and electrochemical testing data. See DOI: https://doi.org/10.1039/d5sc09680d.

Acknowledgements

References

1 X. Yang, X. Wang, Y. Xiang, L. Ma and W. Huang, Asymmetric electrolytes design for aqueous multivalent metal ion batteries, *Nano-Micro Lett.*, 2023, **16**, 51.

2 Z. Pan, X. Liu, J. Yang, X. Li, Z. Liu, X. J. Loh and J. Wang, Aqueous rechargeable multivalent metal-ion batteries: Advances and challenges, *Adv. Energy Mater.*, 2021, **11**, 2100608.

3 J. Wei, P. Zhang, J. Sun, Y. Liu, F. Li, H. Xu, R. Ye, Z. Tie, L. Sun and Z. Jin, Advanced electrolytes for high-performance aqueous zinc-ion batteries, *Chem. Soc. Rev.*, 2024, **53**, 10335–10369.

4 L. Blanc, D. Kundu and L. Nazar, Scientific challenges for the implementation of Zn-ion batteries, *Joule*, 2020, **4**, 771–799.

5 C. Kao, C. Ye, J. Hao, Y. Chen, S. Zhang and S. Qiao, Achieving high energy density in aqueous zinc-ion batteries, *Adv. Energy Mater.*, 2025, 2501201.

6 J. Zhu, X. Ge, Z. Peng, L. Pan, Z. Peng, Y. Jiang, W. Meng, Z. Zhang, N. Zhao, B. Li, L. Dai, L. Wang and Z. He, Interfacial regulation for zinc metal anode of aqueous zinc-ion battery, *Green Energy Environ.*, 2025, **10**, 689–708.

7 Q. Zhang, J. Luan, L. Fu, S. Wu, Y. Tang, X. Ji and H. Wang, The three-dimensional dendrite-free zinc anode on a copper mesh with a zinc-oriented polyacrylamide electrolyte additive, *Angew. Chem., Int. Ed.*, 2019, **58**, 15841–15847.

8 H. Lu, J. Hu, X. Wei, K. Zhang, X. Xiao, J. Zhao, Q. Hu, J. Yu, G. Zhou and B. Xu, A recyclable biomass electrolyte towards green zinc-ion batteries, *Nat. Commun.*, 2023, **14**, 4435.

9 Q. Yang, Q. Li, Z. Liu, D. Wang, Y. Guo, X. Li, Y. Tang, H. Li, B. Dong and C. Zhi, Dendrites in Zn-based batteries, *Adv. Mater.*, 2020, **32**, 2001854.

10 C. Chen, Z. Long, X. Du, L. Li, Q. Liang, D. Chao and D. Li, Interfacial ionic effects in aqueous zinc metal batteries, *Energy Storage Mater.*, 2024, **71**, 103571.

11 H. Yan, S. Li, J. Zhong and B. Li, An electrochemical perspective of aqueous zinc metal anode, *Nano-Micro Lett.*, 2023, **16**, 15.

12 Z. Zhang, B. Xi, X. Ma, W. Chen, J. Feng and S. Xiong, Recent progress, mechanisms, and perspectives for crystal and interface chemistry applying to the Zn metal anodes in aqueous zinc-ion batteries, *SusMat*, 2022, **2**, 114–141.

13 Z. Yao, W. Zhang and J. Zhu, Stabilization of cathode electrolyte interphase for aqueous zinc-ion batteries, *J. Energy Chem.*, 2024, **96**, 359–386.

14 M. Zhang, W. Xu, X. Han, H. Fan, T. Chen, Y. Yang, Y. Gao, C. Zheng, Y. Yang, T. Xiong, Y. Zhang, W. S. V. Lee, W. Wang, H. Pan, Z. G. Yu and J. Xue, Unveiling the mechanism of the dendrite nucleation and growth in aqueous zinc ion batteries, *Adv. Energy Mater.*, 2024, **14**, 2303737.

15 L. Wang, C. Shen, C. Huang, J. Chen and J. Zheng, Regulating the electrical double layer with supramolecular cyclodextrin anions for dendrite-free zinc electrodeposition, *ACS Nano*, 2023, **17**, 24619–24631.

16 Y. Lv, M. Zhao, Y. Du, Y. Kang, Y. Xiao and S. Chen, Engineering a self-adaptive electric double layer on both electrodes for high-performance zinc metal batteries, *Energy Environ. Sci.*, 2022, **15**, 4748–4760.

17 C. Huang, X. Zhao, S. Liu, Y. Hao, Q. Tang, A. Hu, Z. Liu and X. Chen, Stabilizing zinc anodes by regulating the electrical double layer with saccharin anions, *Adv. Mater.*, 2021, **33**, 2100445.

18 D. Feng, Y. Jiao and P. Wu, Guiding Zn uniform deposition with polymer additives for long-lasting and highly utilized zn metal anodes, *Angew. Chem., Int. Ed.*, 2023, **62**, e202314456.

19 M. Peng, X. Tang, K. Xiao, T. Hu, K. Yuan and Y. Chen, Polycation-regulated electrolyte and interfacial electric fields for stable zinc metal batteries, *Angew. Chem., Int. Ed.*, 2023, **135**, e202302701.

20 H. Peng, D. Wang, X. Wang, W. Miao, J. Zeng, B. Tao, Y. Li, Y. Tang and G. Ma, Coupling solvation structure regulation

and interface engineering *via* reverse micelle strategy toward highly stable zn metal anode, *Adv. Funct. Mater.*, 2025, **35**, 2417695.

21 R. Luo, X. Zheng, T. Jiang, D. Shen, M. Wang, M. Ali, H. Liu, Z. Zhang, Y. Feng, S. Hazoor, P. Tong and W. Chen, Reshaping electrical double layer *via* synergistic dual additives for Ah-level zinc battery, *Adv. Energy Mater.*, 2025, 2501658.

22 C. Huang, X. Zhao, Y. Hao, Y. Yang, Y. Qian, G. Chang, Y. Zhang, Q. Tang, A. Hu and X. Chen, Selection criteria for electrical double layer structure regulators enabling stable Zn metal anodes, *Energy Environ. Sci.*, 2023, **16**, 1721–1731.

23 C. Huang, D. Zhu, X. Zhao, Y. Hao, Y. Yang, Y. Qian, G. Chang, Q. Tang, A. Hu and X. Chen, High-entropy-inspired multicomponent electrical double layer structure design for stable zinc metal anodes, *Angew. Chem., Int. Ed.*, 2024, **63**, e202411427.

24 R. Li, M. Li, Y. Chao, J. Guo, G. Xu, B. Li, Z. Liu and C. Yang, YanYu, Hexaoxacyclooctadecane induced interfacial engineering to achieve dendrite-free Zn ion batteries, *Energy Storage Mater*, 2022, **46**, 605–612.

25 X. Xiao, X. Ye, Z. Wu, X. Wu, J. Yu, L. Gu and S. Liu, Trace small molecular/nano-colloidal multiscale electrolyte additives enable ultra-long lifespan of zinc metal anodes, *Adv. Mater.*, 2024, **36**, 2408706.

26 X. Wu, Y. Xia, S. Chen, Z. Luo, X. Zhang, Y. Lu, H. Pan, B. B. Xu, M. Yan and Y. Jiang, Transient zwitterions dynamics empowered adaptive interface for ultra-stable Zn plating/stripping, *Small*, 2024, **20**, 2306739.

27 Y. Ding, X. Zhang, T. Wang, B. Lu, Z. Zeng, Y. Tang, J. Zhou and S. Liang, A dynamic electrostatic shielding layer toward highly reversible Zn metal anode, *Energy Storage Mater.*, 2023, **62**, 102949.

28 Z. Zha, T. Sun, D. Li, T. Ma, W. Zhang and Z. Tao, Zwitterion as electrical double layer regulator to in-situ formation of fluorinated interphase towards stable zinc anode, *Energy Storage Mater.*, 2024, **64**, 103059.

29 Y. Deng, Z. Xiao, W. Xu, Y. Wang, Z. Peng, L. Fei and T. Wang, Moderate yet reversible oligozwitterion adsorption unlocks stable zinc-ion batteries, *Adv. Funct. Mater.*, 2025, e09652.

30 K. Liu, M. Sun, Y. Wu, T. Zhang, A. Zhu, S. Bu, C. Luan, K. Liu, Y. Zhou, D. Lin, S. Wu, C. S. Lee, B. Huang, G. Hong and W. Zhang, Binary electrolyte additive-reinforced interfacial molecule adsorption layer for ultra-stable zinc metal anodes, *Adv. Mater.*, 2025, **37**, 2420079.

31 M. Su, H. Dou, J. Yan, S. Liu, M. Xu, C. Liu, X. Wang and Z. Chen, Multisite cooperative regulation of solvation and interface *via* dynamic additive engineering for highly reversible zinc batteries, *Angew. Chem., Int. Ed.*, 2025, **64**, e202511685.

32 G. Duan, Y. Wang, B. Luo, L. Sun, S. Zheng, J. Huang and Z. Ye, Taurine-mediated dynamic bridging strategy for highly stable Zn metal anode, *Energy Storage Mater.*, 2023, **61**, 102882.

33 C. Huang, J. Mao, S. Li, W. Zhang, X. Wang, Z. Shen, S. Zhang, J. Guo, Y. Xu, Y. Lu and J. Lu, Amphoteric

polymer strategy with buffer-adsorption mechanism for long-life aqueous zinc ion batteries, *Adv. Funct. Mater.*, 2024, **34**, 2315855.

34 Q. Shao and S. Jiang, Molecular understanding and design of zwitterionic materials, *Adv. Mater.*, 2015, **27**, 15–26.

35 H. Yu, D. Chen, X. Ni, P. Qing, C. Yan, W. Wei, J. Ma, X. Ji, Y. Chen and L. Chen, Reversible adsorption with oriented arrangement of a zwitterionic additive stabilizes electrodes for ultralong-life Zn-ion batteries, *Energy Environ. Sci.*, 2023, **16**, 2684–2695.

36 Z. Meng, Y. Jiao and P. Wu, Alleviating side reactions on Zn anodes for aqueous batteries by a cell membrane derived phosphorylcholine zwitterionic protective layer, *Angew. Chem., Int. Ed.*, 2023, **62**, e202307271.

37 B. Wang, C. Guan, Q. Zhou, Y. Wang, Y. Zhu, H. Bian, Z. Chen, S. Zhang, X. Tan, B. Luo, S. Tang, X. Meng and C. Zhang, Screening anionic groups within zwitterionic additives for eliminating hydrogen evolution and dendrites in aqueous zinc ion batteries, *Nano-Micro Lett.*, 2025, **17**, 314.

38 Q. Shao and S. Jiang, Influence of charged groups on the properties of zwitterionic moieties: A molecular simulation study, *J. Phys. Chem. B*, 2014, **118**, 7630–7637.

39 M. Chuai, H. Tong, Z. Yang, S. Deng, M. Wu, J. Xing and G. Chai, Design of a P–O–M (M = Mn, Zn) d-pπ backbonding electrolyte additive for 40 Ah electrolytic Zn–MnO$_2$ batteries, *J. Am. Chem. Soc.*, 2025, 31591–31602.

40 W. Yang, Y. Yang, H. Yang and H. Zhou, Regulating water activity for rechargeable zinc-ion batteries: Progress and perspective, *ACS Energy Lett.*, 2022, **7**, 2515–2530.

41 Y. Deng, C. Xing, C. Li, Y. Zhou, Z. Peng, L. Fei, C. Zhi and T. Wang, Effective water confinement and dual electrolyte–electrode interfaces by zwitterionic oligomer for high-voltage aqueous lithium-ion batteries, *Adv. Funct. Mater.*, 2025, **35**, 2416566.

42 H. Dai, X. Gu, J. Dong, C. Wang, C. Lai and S. Sun, Stabilizing lithium metal anode by octaphenyl polyoxyethylene-lithium complexation, *Nat. Commun.*, 2020, **11**, 643.

43 S. Chen, D. Ji, Q. Chen, J. Ma, S. Hou and J. Zhang, Coordination modulation of hydrated zinc ions to enhance redox reversibility of zinc batteries, *Nat. Commun.*, 2023, **14**, 3526.

44 Y. Xie, S. Feng, J. Gao, T. Cheng and L. Zhang, Modulating the interfacial microenvironment *via* zwitterionic additive for long-cycling aqueous Zn-ion batteries, *Sci. China Mater.*, 2024, **67**, 2898–2907.

45 J. Zhang, Y. Liu, Y. Wang, Z. Zhu and Z. Yang, Zwitterionic organic multifunctional additive stabilizes electrodes for reversible aqueous Zn-ion batteries, *Adv. Funct. Mater.*, 2024, **34**, 2401889.

46 S. Deng, Y. Sun, Z. Yang, M. Wu, H. Tong, X. Nie, Y. Su, J. Li and G. Chai, Zwitterion-separated ion pair dominated additive-electrolyte structure for ultra-stable aqueous zinc ion batteries, *Adv. Funct. Mater.*, 2024, **34**, 2408546.

47 Y. Zhao, S. Guo, M. Chen, B. Lu, X. Zhang, S. Liang and J. Zhou, Tailoring grain boundary stability of zinc-titanium alloy for long-lasting aqueous zinc batteries, *Nat. Commun.*, 2023, **14**, 7080.